Guiding the experimental discovery of magnesium alloys

Richard H. Taylor, Stefano Curtarolo, and Gus L. W. Hart

Phys. Rev. B **84**, 084101 — Published 19 August 2011

DOI: 10.1103/PhysRevB.84.084101

Guiding the experimental discovery of magnesium alloys

Richard H. Taylor[a,b], Stefano Curtarolo[b,⋆], Gus L. W. Hart[a,⋆]
[a] *Department of Physics and Astronomy, Brigham Young University, Provo, Utah 84602, USA*
[b] *Department of Mech. Eng. and Materials Science and Department of Physics, Duke University, Durham NC, USA and*
[⋆] *E-mail: stefano@duke.edu; gus.hart@gmail.com*

Abstract: Magnesium alloys are among the lightest structural materials known and are of considerable technological interest. To develop superior magnesium alloys, experimentalists must have a thorough understanding of the concentration-dependent precipitates that form in a given system; and hence, the thermodynamic stability of crystal phases must be determined. This information is often lacking but can be supplied by first-principles methods. Within the high-throughput framework, AFLOW, T=0 K ground state predictions are made by scanning a large set of known candidate structures for thermodynamic (formation energy) minima. The study presented here encompasses 34 Mg-X systems of interest (X=Al, Au, Ca, Cd, Cu, Fe, Ge, Hg, Ir, K, La, Pb, Pd, Pt, Mo, Na, Nb, Os, Rb, Re, Rh, Ru, Sc, Si, Sn, Sr, Ta, Tc, Ti, V, W, Y, Zn, Zr). Avenues for further investigation are clearly revealed by this work. These include new stable phases predicted in compound-forming systems as well as phases predicted in systems reported to be non-compound-forming.

I. INTRODUCTION

The importance of materials in modern society is difficult to overstate and continues to grow as twenty-first century challenges emerge. Concern over human energy consumption and environmental impact has become urgent in recent years, even making a striking entrance into the public discourse. Paralleling this, the desire for highly efficient materials tailored to specific applications has increased. A great deal of effort has focused on material weight and strength. Light yet durable materials are needed in the automotive and aerospace industries, two sectors that are jointly responsible for a large source of anthropogenic pollutants and a significant portion of global energy consumption[2].

Magnesium (Mg) alloys are among the lightest structural materials known and are used in a variety of applications, particularly in automotive and aerospace manufacturing. The abundance of magnesium is an important practical consideration and suggests that increased consumption could be sustained. Indeed, over the past decade Mg consumption has increased dramatically due in large part to an impetus in the automotive industry for lighter, more energy efficient vehicles. This has been accompanied by an increase of Mg research, and although much progress has been made toward a complete understanding of Mg alloys much remains to be done.

In improving or designing alloys, materials scientists rely on the thermodynamic information in published phase diagrams. This information is found directly through experimental reports and by modeled data (e.g., using the CALPHAD method). However, thermodynamic data for even common alloys is sometimes incomplete. This is due, at least in part, to the difficulty of achieving thermodynamic equilibrium at low temperatures and the inability to make accurate models from incomplete or unreliable experimental data sets. First-principles (*ab initio*) methods provide a powerful tool in this arena and can be used to complete our understanding of the low temperature thermodynamics of alloys.

Ab initio methods have long been recognized as a viable approach to the study of materials and have already been applied to a number of Mg systems (see for example Ref.[3,4]). Accurate formation energy predictions at zero temperature only require details of the crystal structure and composition; and although calculations of this sort are slow compared to very fast models such as cluster expansion, they are not limited to derivative superstructures of a parent lattice. In a *high-throughput* (HT) approach, searches over many crystallographic types can be made, thereby introducing the possibility of making surprising (even off-lattice) predictions. Ground state predictions made in this manner are typically in very good agreement with experimental results as shown by Curtarolo, Morgan, and Ceder[5] in a review of 80 binary systems.

Using the HT framework AFLOW[5–13], we have explored the full composition range of 34 Mg-X binary systems at $T = 0$ K. In the large majority of cases, our calculations are consistent with experimental phases. That is, the ordered phases shown in the phase diagram coincide with the low temperature ground state predictions of the HT approach. In nearly all the remaining cases, the differences between the HT results and phase diagrams are relatively minor (though the differences may still indicate new opportunities for alloy design). Finally, there are some instances of strong disagreement, but they are few. Included in these are three non-compound-forming systems reported here with one or more stable *ab initio* compounds.

The remainder of the paper progresses as follows. After a discussion of the HT methodology and library, systems without *ab initio* compounds are reported. Following this, compound forming systems are summarized and then discussed system by system. These are presented in alphabetical order with tables containing summarizing data related to each. Plots showing formation energy versus atomic percent Mg for each system are also included.

Compound	AB_4[1]	AB_3	A_2B_2	A_2B_2	A_2B_2	A_2B_2
Superlattice	fcc	bcc	bcc	bcc	fcc	fcc
Lattice	monoclinic	monoclinic	orthorhombic	orthorhombic	monoclinic	tetragonal
Space group	C2/m #12	P2/m #10	Cmma #67	Imma #74	C2/m #12	P4/nmm #129
Pearson symbol	mS10	mP4	oS8	oI8	mS8	tP4
Primitive vect.						
$\mathbf{a}_1$/a	(1/2,1/2,0)	(0,-2,0)	(1/2,1/2,1/2)	(3/2,1/2,-1/2)	(-1/2,1,-1/2)	(0,-1/2,-1/2)
$\mathbf{a}_2$/a	(0,5/2,5/2)	(-1,0,-1)	(-1/2,-1/2,1/2)	(1/2,3/2,1/2)	(-1/2,1/2,-1)	(0,-1/2,1/2)
$\mathbf{a}_3$/a	(1/2,1,3/2)	(1/2,5/2,-1/2)	(2,-2,0)	(-1/2,-3/2,1/2)	(0,-2,2)	(-2,0,0)
Atomic Positions						
A1	(0,0,0)	(0,0,0)	(0,0,0)	(0,0,0)	(0,0,0)	(0,0,0)
A2	—	—	(1/2,1/2,3/4)	(1/4,3/4,1/2)	(0,0,3/4)	(1/2,1/2,3/2)
B1	(0,1/5,0)	(3/4,1/2,0)	(0,0,1/2)	(1/2,1/2,0)	(0,0,1/4)	(0,0,1/2)
B2	(0,2/5,0)	(1/2,0,0)	(1/2,1/2,1/4)	(3/4,1/4,1/2)	(0,0,1/2)	(1/2,1/2,1/4)
B3	(0,3/5,0)	(1/4,1/2,0)	—	—	—	—
B4	(0,4/5,0)	—	—	—	—	—
AFLOW label	"f52"	"73/75"	"71"	"80"	"17"	"14"

TABLE I: Crystallographic data for unrelaxed bcc-, fcc-, hcp-derived prototypes arising in our study.

II. METHOD

In the HT approach used here, the ground state profile of a binary system is studied by a correlated brute force search. Formation energies (calculated with respect to the most stable structure of the pure elements) are obtained for all common prototypes for the class under investigation (i.e., Mg-X) as well as for a large number of enumerated derivative superstructures[14]. This procedure has given reasonable results for a large number of systems as described in Ref.[5]. Here it was shown that the probability of reproducing the correct ground state, if well defined, not ambiguous, and present in the list of prototypes was $\eta_c^\star \sim 96.7\%$ (*"reliability of the method"*, Eq. (3) of Ref.[5]).

The accuracy of the method can be quantified in a similar manner for the systems included in this report. As an upper bound we may consider the correct ground state to be obtained when the experimental phase is predicted close to the energy of the tie line. In particular, accurate predictions will include lowest energy phases at a given composition that are in agreement with the experimental phase but do not contribute to the convex hull topology (are slightly above the tie line) or are only a few meV above a related *ab initio* ground state. In the latter case, stabilization at finite temperature may be due to, for instance, vibrational entropy. Finally, in this estimation of the methods accuracy, only unambiguously defined phases present in the list of prototypes are considered as valid comparisons.

The total number of *potential structure comparisons* (i.e., all instances of experimentally determined intermetallic phases in the systems included in this study) is 58. Some of these were not available as comparison structures due to either ambiguity in the definition, unknown prototypes, or large unit cells. When these are excluded, we find the *total available structure comparisons* ($N_t = 45$). The available structure comparisons can be divided into those with *exact ab initio agreement* ($N_e = 38$), *possible/likely ab initio agreement* ($N_p = 7$) (small deviations from the convex hull energy likely due to i) calculation error and/or ii) entropic effects), and *clear disagreement* ($N_d = 1$).

Let the total number of non-compound-forming systems ($N_{ti} = 12$) be divided into *ab initio* agreements ($N_{ai} = 11$) and disagreements ($N_{di} = 1$). (The Mg-Zr and Mg-Tc systems are excluded due to a lack of reliable experimental data across the entire composition range.) A lower bound (LB) on the accuracy of our method in the Mg-X systems studied here is provided by the ratio of exact *ab initio* agreement to the number of available structure comparisons:

$$\eta_{\rm LB} = \frac{N_e + N_{ai}}{N_t + N_{ti}} \approx 86.0\% \tag{1}$$

We find the upper bound (UB) on the reliability of our method by the ratio of correct compounds including possible/likely *ab initio* agreement and non-compound-forming systems ($N_e + N_p + N_{ai}$) to the total number of available structure and non-compound-forming system comparisons ($N_t + N_{ti}$):

$$\eta_{UB} \equiv \frac{N_e + N_p + N_{ai}}{N_t + N_{ti}} \approx 98.2\% \tag{2}$$

Therefore, the accuracy of the method (η_c) in reproducing the correct ground state of the included systems - if present in the list of prototypes and unambiguously defined - is estimated between $\eta_{\rm LB} \approx 86.0\%$ and $\eta_{\rm UB} \approx 98.2\%$:

$$86.0\% \leq \eta_c \leq 98.2\% \tag{3}$$

Of course there is no guarantee that the *true* ground states of a system will be found among the common experimentally observed structures or among small-unit-cell derivative structures. Nevertheless, even if it is impossible to rule out the existence of an alternate ground state, this procedure (searching many enumerated derivative structures and exploring common and related experimentally reported structures) is expected to give a reasonable balance between HT speed and scientific accuracy to determine the $T = 0\,K$ ground states of Mg-X systems.

Calculations were performed within the AFLOW framework with *ab initio* calculations of the energies given by the VASP software[15]. We mainly used projector augmented wave (PAW) pseudopotentials[16] and the exchange-correlation functionals parameterized by Perdew, Burke and Ernzerhof (PBE)[17] for the generalized gradient approximation (GGA) (exceptions to this are described in the next section). The energies were calculated at zero temperature (K) and pressure, so that energies and enthalpies coincide, with spin polarization and without zero-point motion or lattice vibrations. Zero-point motion is negligible in this study because we do not consider alloys with the lightest elements (e.g., H, Li). All crystal structures were fully relaxed (cell volume and shape, and atomic positions). Numerical convergence to about ∼1 meV/atom was ensured by a high energy cutoff (30% higher than the highest energy cutoff for the pseudopotentials of the components) and dense 6000-8000 **k**-point Monkhorst-Pack meshes.

A. Structure library

The energies of around 250 crystal structures were calculated for each of the Mg-X systems studied. In addition to the 176 configurations described in[5], these included all the symmetrically-distinct hcp-, bcc-, fcc-based superstructures[14] with up to four atoms per cell, and the prototypes A5, A6, A7, A8, A9, A11, A13, A12, B20, C1, C_b, C36, $D0_{19}$, $D0_{21}$, $D5_{19}$, $D8_c$, $D8_{11}$, $AuMg_2$, Al_2Zr_4, Al_3Zr_2, $Au_{3\pm x}Mg$, CdTi, $CuPt_7$, Cu_3Ti_2, Ga_2Hf, Ga_4Ni, Ga_3Pt_5, Ga_4Ti_5, Hg_2Pt, ITl, InTh, LiB-MS1/2[9,10,12,18,19], $Mg_{44}Rh_7$, $Mg38Sr_9$, $Mn_{23}Th_6$, $NbNi_8(Pt_8Ti)$, $Ni_{17}Th_2$, $NiTi_2$, SeTl and V_4Zn_5. The additional prototypes were considered because they are common or related to Mg alloys[20,21]. Crystallographic data for less familiar prototypes arising in our study (relaxed and unrelaxed) are given in Tables I, XXVII, and XXVIII.

The solute elements considered in this study are the following: Al, Au, Ca, Cd, Cu, Fe, Ge, Hg, Ir, K, La, Mo, Na, Nb, Os, Pb, Pd, Pt, Rb, Re, Rh, Ru, Sc, Si, Sn, Sr, Ta, Tc, Ti, V, W, Y, Zn, and Zr. This includes most of the transition metals and several other alloys including some of industrial importance (e.g., Al, Ca). Although also systems of interest, Ag-Mg, Hf-Mg, In-Mg, and Li-Mg were not included because one or more of the authors have already reported HT *ab initio* data on these systems[5,10,11,22].

In the systems Al-, Ge-, and Si-Mg, anomalously low energies (many meV below the next lowest energies) were obtained for the Be_2Zn structure. The topology of the convex hull was in these instances entirely determined by the Be_2Zn phase. This lead to results in complete contradiction of experiment. Furthermore, the relaxed atomic volumes were found inexplicably lower than the constituent element values and neighboring structures. For the Al-, Ge-, and Si-Mg systems, the combination of PBE functionals and VASP apparently lead to the erroneous results. When the local density approximation (LDA) or Perdew and Wang[23] (PW) functionals were used, reasonable results were obtained. These were further corroborated by linearized augmented plane-wave (LAPW) calculations using the WIEN2K package[24]. In these three cases, the Be_2Zn structure had positive formation energy and reasonable equilibrium atomic volumes. Experimental ground states were also largely confirmed. Therefore, the results reported in this paper for Al-, Ge-, and Si-Mg are based on PW functionals. Further discussion of the unusual behavior exhibited when the PBE parameterization is used is beyond the scope of this paper.

III. RESULTS AND DISCUSSION

A. Non-compound-forming systems

No stable compounds were found in the following immiscible systems: Fe-Mg, K-Mg, Mg-Mo, Mg-Nb, Mg-Os, Mg-Rb, Mg-Re, Mg-Ta, Mg-Ti, Mg-V, and Mg-W. Non-compound-forming systems predicted by our study (identified by a complete lack of phases with negative formation energies) were in every case also reported to be without intermediate phases experimentally. The converse, however, was not always true. Several systems reported to be non-compound-forming produced thermodynamically stable compounds. These systems, Na-, Tc-, and Zr-Mg, are included in what follows (see also Table II). This ostensible disagreement with experiment is not altogether surprising; Na is reactive and experimental data for the Mg-Tc and Mg-Zr systems is incomplete.

System	**Composition**	**Compound**	**Enthalpy** (meV/atom)
Mg-Na	Mg_3Na_2	Al_3Zr_2	-223.9
Mg-Tc	$MgTc_2$	$C11_b$	-15.8
	Mg_3Tc_4	Cu_4Ti_3	-20.2
	MgTc	B11	-22.4
Mg-Zr	Mg_3Zr_4	Cu_4Ti_3	-31.6
	MgZr	B11	-31.3

TABLE II: Non-compound-forming systems with *ab initio* compounds. The enthalpy of the *ab initio* ground state (columns one and two) is reported in column three.

B. Systems with *ab initio* compounds

All low-temperature experimental and $T = 0\,\mathrm{K}$ *ab initio* ground states are described by individual system tables (a summary of *ab initio*/experimental disagreement is given in Table XXVI). In the system tables (Tables III-XXV), compounds are reported in order of increasing Mg content, with Mg concentration given in the first column, experimental results given in the second column, and *ab initio* results given in the third column. Relative formation energies may be given in instances of a) very close (in energy) competing phases, b) when experimental phases are many meV/atom above the *ab initio* ground state, or c) when an *ab initio* ground state does not exist. In non-compound-forming systems with *ab initio* ground states, the formation energy is given. In systems without known phase diagrams, experimental results are indicated by a dash (—) when compared to *ab initio* results. Experimental phases with unit-cells too large to be accurately studied by HT *ab initio* methods are indicated by three stars (***). If the experimental compound is undetermined, this is denoted by *unknown*. Structures marked with an asterisk (e.g., $A_2B^{\star}$-65) are relaxed prototypes and are described in the Tables I,XXVII, and XXVIII. If necessary, Pearson symbols and space group number are listed in parentheses.

Al-Mg *(Aluminum-Magnesium)*

No simple experimental compounds exist in the Al-Mg system. Two complex low-temperature phases are reported in experimental phase diagrams: $Al_{12}Mg_{17}$-A12, and $Al_{45}Mg_{28}$-β. We did not calculate formation energy for the β structure due to the large unit cell and partial occupation of sites. Thus, although a stable phase is predicted by *ab initio* calculations at composition Al_2Mg, the system must be investigated further to more accurately predict phase(s) at Mg concentration less than ∼50%. It is known that the β phase undergoes a Martensitic transformation to another structure (possibly a distortion of β) at low temperature[21]. In agreement with experiment, the A12 phase is a thermodynamic minimum.

Al-Mg system

Comparison of low temperature phases		
Composition % Mg	Experimental results[21,25–48]	*Ab initio* results (Fig. 1)
33.3	*two-phase region*	Ag_2Mg-C14/C36 C15 ∼5.20 meV/atom *above* C14
∼38.4	$Al_{45}Mg_{28}$	***
∼58.6	$Al_{12}Mg_{17}$-A12	A12

TABLE III: The Al-Mg system.

Au-Mg *(Gold-Magnesium)*

The Au-Mg phase diagram is incomplete, particularly on the Au-rich side. An *ab initio* phase is predicted in this region with the $HfPd_5$ structure reported in Ref.[10]. We evaluated the off-stoichiometry orthorhombic phases - $AuMg_{3-x}$ (oS160, #63) and $AuMg_{3+x}$ (oS64, #63) - and the $D0_{23}$ phase at composition Au_3Mg. The orthorhombic phase formation energies differ by less than 1 meV - within numerical error - and are thus both reported as the ground state. The phase with structure $D0_{23}$ is a few meV above the stable compounds $AuMg_{3-x}$ and $AuMg_{3+x}$. Indeed, $D0_{23}$ is not expected to be stable at $T = 0\,\mathrm{K}$: experiment reports the phase only forming above ∼ 645°C[21].

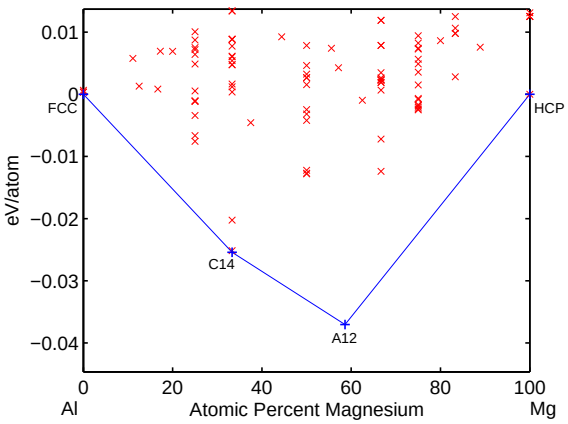

FIG. 1. Al-Mg convex hull.

On the Mg-rich side, the experimental phases AuMg-B2, $AuMg_2$ (oP108, #62), and $AuMg_{2.82}$-$D0_{21}$ are stable. An additional *ab initio* phase with the Au_3Mg_5-$D8_m$ structure is also stable.

Au-Mg system

Comparison of low temperature phases		
Composition % Mg	Experimental results[21,49–51]	*Ab initio* results (Fig. 2)
16.6	*solid solution*	$HfPd_5$[10]
25.0	$Au_{3-x}Mg/Au_{3+x}Mg$ Au_3Mg-$D0_{23}$ *high-temperature*	$Au_{3-x}Mg/Au_{3+x}Mg$ $D0_{23}$ ∼3.4 meV/atom *above* $Au_{3-x}Mg$
50.0	AuMg-B2	$B2/L1_0$
62.5	*two-phase region*	Au_3Mg_5-$D8_m$
66.6	$AuMg_2$	$AuMg_2$
∼75.0	$AuMg_3$-$D0_{21}$	$D0_{21}$

TABLE IV: The Au-Mg system.

Ca-Mg *(Calcium-Magnesium)*

Ca-Mg is a simple eutectic system having one intermetallic compound. The experimental phase forms at composition $CaMg_2$ with the C14 Laves structure. Experimental phase diagrams show the phase melts congru-

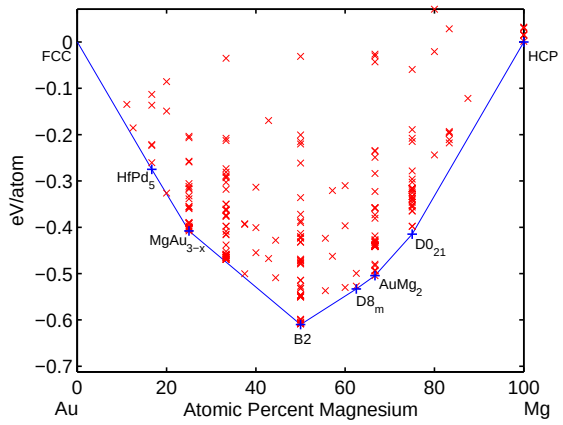

FIG. 2. Au-Mg convex hull.

ently with no homogeneity field. *Ab initio* calculations reveal a single ground state at the same composition with the C14 structure. The two additional Laves phase polytypes C36 and C15 are close in formation energy. The close structural similarity between these close-in-energy phases suggests dominant short-range interactions.

Ca-Mg system

Comparison of low temperature phases		
Composition % Mg	Experimental results[21,52–58]	*Ab initio* results (Fig. 3)
66.6	$CaMg_2$-C14	C14 C36 ∼2.3 meV/atom C15 ∼4.2 meV/atom *above* C14

TABLE V: The Ca-Mg system.

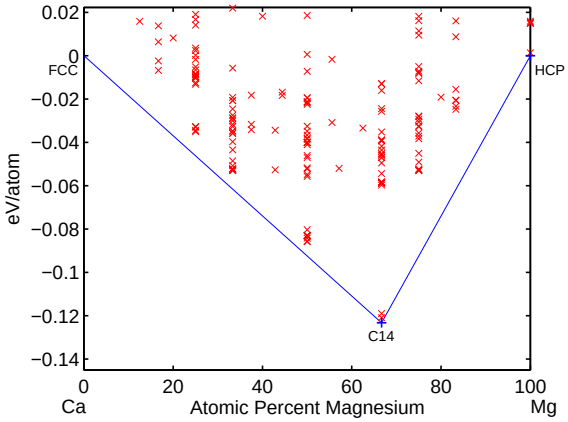

FIG. 3. Ca-Mg convex hull.

Cd-Mg *(Cadmium-Magnesium)*

Experimental phase diagrams indicate intermetallic compounds with structures Cd_3Mg-$D0_{19}$, CdMg-B19, and $CdMg_3$-$D0_{19}$. *Ab initio* ground states exist at the same compositions with identical structures. An additional phase is predicted at composition $CdMg_2$ with the $InMg_2$ structure.

Cd-Mg system

Comparison of low temperature phases		
Composition % Mg	Experimental results[21,59–74]	*Ab initio* results (Fig. 4)
∼25.0-32.0	Cd_3Mg-$D0_{19}$	$D0_{19}$
∼38.0-60.0	AuCd-B19	B19
66.6	*two-phase region*	$InMg_2$
∼65.0-82.0	$CdMg_3$-$D0_{19}$	$D0_{19}$

TABLE VI: The Cd-Mg system.

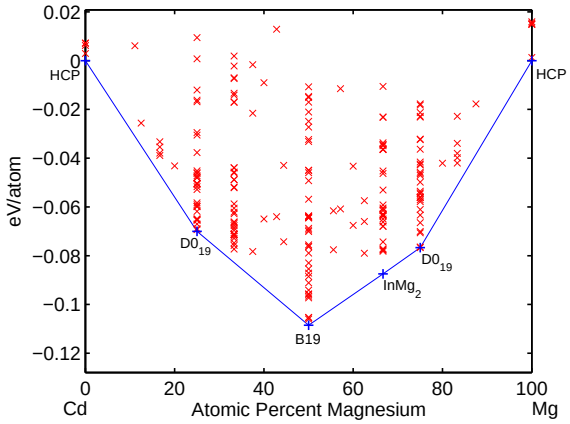

FIG. 4. Cd-Mg convex hull.

Cu-Mg *(Copper-Magnesium)*

Ab initio ground states in the Cu-Mg system agree with experiment. Experimental phase diagrams show intermetallic compounds at compositions Cu_2Mg and $CuMg_2$ with the C15 and C_b structures respectively. According to *ab initio* calculations, the Cu_2Mg-C15 structure is close in energy to the two other Laves phase polytypes, C36 and C14, suggesting weak long range interactions.

Experimental phase diagrams show the phases melt congruently. Thus, given the agreement of the T = 0 K *ab initio* predictions, the phases may be stable from T = 0 K to the liquidus line.

Cu-Mg system

Comparison of low temperature phases		
Composition % Mg	Experimental results[21,75–79]	*Ab initio* results (Fig. 5)
∼31-35.3	Cu_2Mg-C15	C15 C36 ∼0.9 meV/atom C14 ∼2.1 meV/atom *above* C15
66.6	$CuMg_2$-C_b	C_b

TABLE VII: The Cu-Mg system.

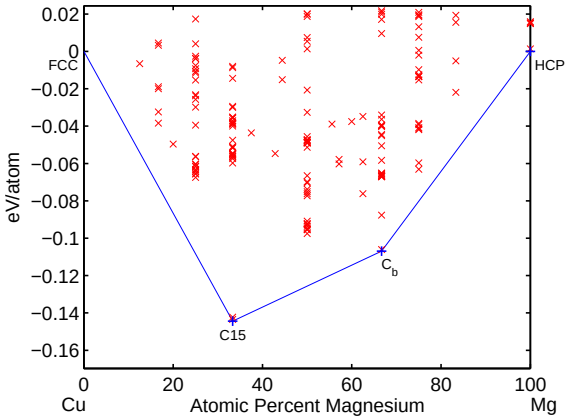

FIG. 5. Cu-Mg convex hull.

Ge-Mg *(Germanium-Magnesium)*

A single *ab initio* compound is predicted to be thermodynamically stable in the Ge-Mg system. The phase, Ge_2Mg-C1, is in agreement with experimental data.

Ge-Mg system

Comparison of low temperature phases		
Composition % Mg	Experimental results[21,80–83]	*Ab initio* results (Fig. 6)
66.6	Ge_2Mg-C1	C1

TABLE VIII: The Ge-Mg system.

Hg-Mg *(Mercury-Magnesium)*

Experimental phases are verified by *ab initio* calculations with differences at compositions Hg_2Mg and $HgMg_3$. The unidentified phase at composition Hg_2Mg_5 was not supported by *ab initio* results (no stable compound was found at this composition). However, this result is inconclusive, as only a small number of structures with the appropriate composition exist in the database.

The phases at compositions Hg_2Mg and $HgMg_3$ are not thermodynamically stable at T = 0 K, according to *ab initio* data, although phases with different structures are predicted relatively close to the tie line. The Hg_2Mg-C_c and $HgMg_3$-$D0_{19}$ phases are predicted instead of $C11_b$ and $D0_{19}$, respectively.

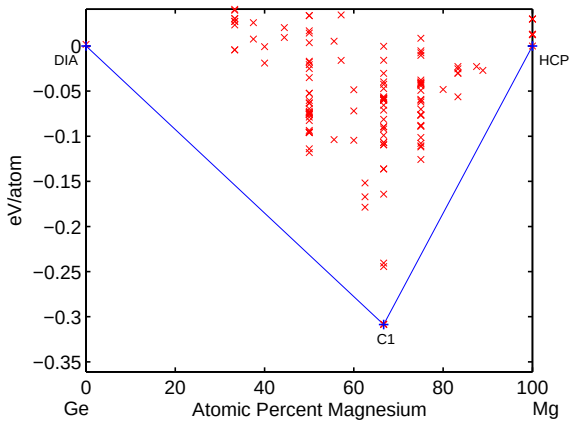

FIG. 6. Ge-Mg convex hull.

Hg-Mg system

Comparison of low temperature phases		
Composition % Mg	Experimental results[21,84–86]	*Ab initio* results (Fig. 7)
33.3	Hg_2Mg-$C11_b$	*two-phase region* C_c ∼2.0 meV/atom *above tie line* C37 ∼21.4 meV/atom $C11_b$ ∼22.0 meV/atom *above* C_c
50.0	HgMg-B2	B2
62.5	Hg_3Mg_5-$D8_8$	$D8_8$
66.6	$HgMg_2$-C37	C37
71.4	Hg_2Mg_5 *unknown*	*two-phase region*
75.0	$HgMg_3$-$D0_{18}$	*two-phase region* $D0_{19}$ ∼3.8 meV/atom *above tie line* $D0_{18}$ ∼28.5 meV/atom *above* $D0_{19}$

TABLE IX: The Hg-Mg system.

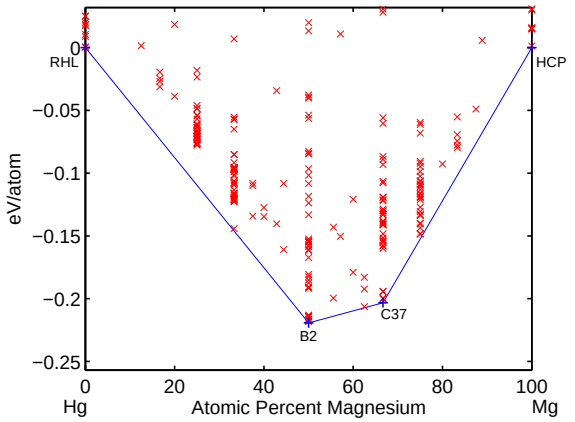

FIG. 7. Hg-Mg convex hull.

Ir-Mg *(Iridium-Magnesium)*

Although Ir is rare and costly it has remarkable physical and chemical properties[87]. Yet the very same properties that make it a material of interest (high melting point, resistance to corrosion, etc.) make the study of its alloys challenging.

Ir-Mg is no exception and the experimental phase diagram for this system is not complete. Data is especially sparse at low temperatures, perhaps due to the high-melting temperature of Ir. Experimental Ir-rich phases are unknown; the most Ir-rich phase is found at composition $IrMg_3$ with the $D0_{21}$ structure.

Given the lack of experimental data on the Ir-rich side, *ab initio* predictions are particularly interesting. Two *ab initio* Ir-rich phases are found: the fcc derived Ca_7Ge structure and an hcp-derived prototype[13], $Re_3Ru^{\star}$-124 described in Structure Table 2. An fcc derived structure with A_2B_2 stacking along the [311] direction is thermodynamically stable at composition IrMg.

We are able to report with less certainty the Mg-rich phases. The experimental phase $Mg_{44}Ir_7$ (cF408, #216) was only roughly evaluated because of the large unit cell size. The k-point mesh was course by necessity, and it is likely the cell was not able to reach equilibrium volume. Nevertheless, the energy was found negative ($\sim$ 40meV above the tie line). The structural details of the reported phase at composition $IrMg_4$ are not known, and thus the absence of a stable *ab initio* phase at this composition is indeterminate. Finally, the stability of the $IrMg_{2.82}$-$D0_{21}$ phase by *ab initio* calculations confirms experiment.

Ir-Mg system

Comparison of low temperature phases		
Composition % Mg	Experimental results[21,88]	*Ab initio* results (Fig. 8)
12.5	—	Ca_7Ge
25.0	—	$Re_3Ru^{\star}$-124† Ir_3Mg-"$L1_3$"[5] ~62.3 meV/atom *above* $Re_3Ru^{\star}$-124
50.0	—	$FCC^{[311]}_{A2B2}$ †
75.0	$IrMg_3$-$D0_{21}$	$D0_{21}$
80.0	$IrMg_4$ *unknown*	*two-phase region* $D1_a$ ~65.0 meV/atom *above tie line.*
86.2	Ir_7Mg_{44}	Ir_7Mg_{44} ~40.0 meV/atom *above tie line*

TABLE X: The Ir-Mg system. (†) See Structure Tables for crystallographic description.

La-Mg *(Lanthanum-Magnesium)*

Stable *ab initio* phases agree with the La-Mg experimental phases LaMg-B2, $LaMg_3$-$D0_3$ and $Ni_{17}Th_2$. The structural data for the experimental phase at composition $LaMg_{12}$ is not complete, although a phase with a $CeMg_{12}$(II)-type structure has been proposed[21]. *Ab initio* calculations were not performed in this case due to the large unit cell size. La-rich phases have not been observed experimentally; however, an *ab initio* phase was predicted at composition La_7Mg with the Ca_7Ge structure.

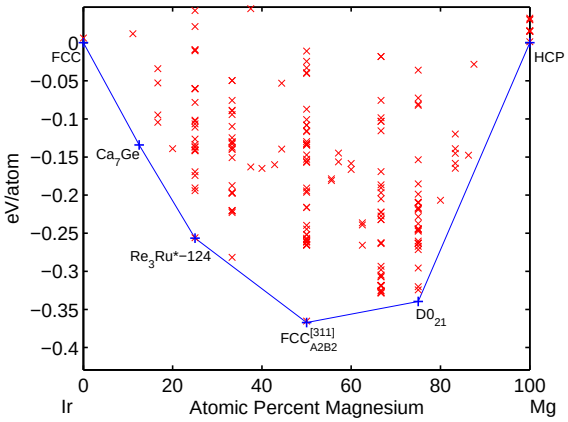

FIG. 8. Ir-Mg convex hull.

La-Mg system

Comparison of low temperature phases		
Composition % Mg	Experimental results[21,89–94]	*Ab initio* results (Fig. 9)
12.5	*two-phase region*	Ca_7Ge
50.0	LaMg-B2	B2 NiTi ~4.4 meV/atom *above* B2
75.0	$LaMg_3$-$D0_3$	$D0_3$ $D0_{19}$ ~42.3 meV/atom *above* $D0_3$.
~89.5	$Ni_{17}Th_2$	$Ni_{17}Th_2$
~91.67-92.86	$LaMg_{12}$ *unknown/* *CeMg12 (II)*	*two-phase region* ***

TABLE XI: The La-Mg System.

Mg-Na *(Magnesium-Sodium)*

No intermetallic phases have been found in the Mg-Na system by experimental investigation[21]. An *ab initio* ground state is predicted at composition Mg_3Na_5 with the Al_3Zr_2-type structure (oF40, #43). Additional compounds with negative formation energies are found at compositions $MgNa_3$, Mg_2Na_3, and Mg_3Na_2 with structures $FCC^{[111]}_{AB3}$ (4 atom unit cell, fcc derived supercell with stacking along [111]), and Mg_3Na_2-C33.

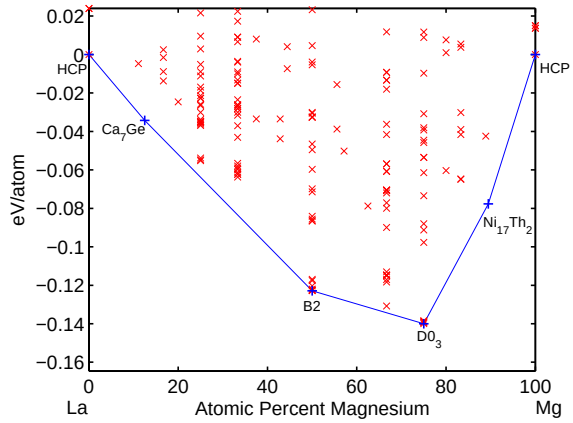

FIG. 9. La-Mg convex hull.

Mg-Na system

Comparison of low temperature phases		
Composition % Mg	Experimental results[21]	*Ab initio* results (Fig. 10)
60.0	*non-compound-forming*	Al_3Zr_2 ∼-223.9 meV/atom
		C33 ∼199.5 meV/atom *above* Al_3Zr_2

TABLE XII: The Mg-Na system.

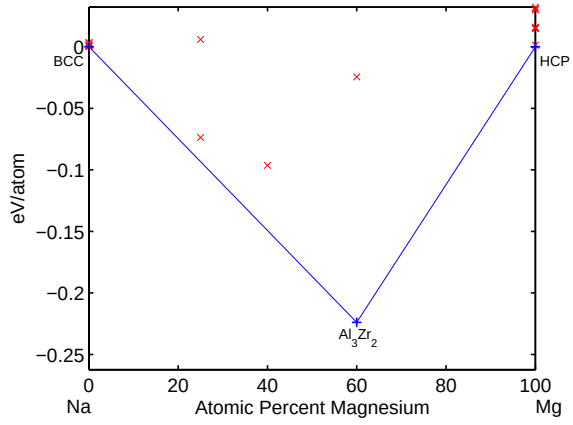

FIG. 10. Mg-Na convex hull.

Mg-Pb *(Magnesium-Lead)*

Experimental phase diagrams indicate a single intermetallic compound at composition Mg_2Pb with the fluorite structure, C1. *Ab initio* calculations reveal additional phases $MgPb_3$-75 (see Structure Table 2 for description), MgPb-$L1_1$, and Mg_3Pb-$L1_2$. A metastable phase with the $L1_2$ structure has been observed by splat cooling[95]; however, the phase decomposed into Mg(hcp)+Mg_2Pb-C1 when kept at room temperature. The stability of $L1_2$ at T=0 K predicted by *ab initio* calculations suggests the phase may be stable at below-room temperature.

Mg-Pb system

Comparison of low temperature phases		
Composition % Mg	Experimental results[21,96–103]	*Ab initio* results (Fig. 11)
25.0	*two-phase region*	AB_3-75[†]
50.0	*two-phase region*	MgPb-$L1_1$
66.6	Mg_2Pb-C1	C1
∼77.0-84.0	Mg_3Pb-$L1_2$ *(metastable)*	$L1_2$ Co_3V (hP24 *phase*) ∼2.4 meV/atom *above* $L1_2$

TABLE XIII: The Mg-Pb System. (†) See Structure Tables for crystallographic description.

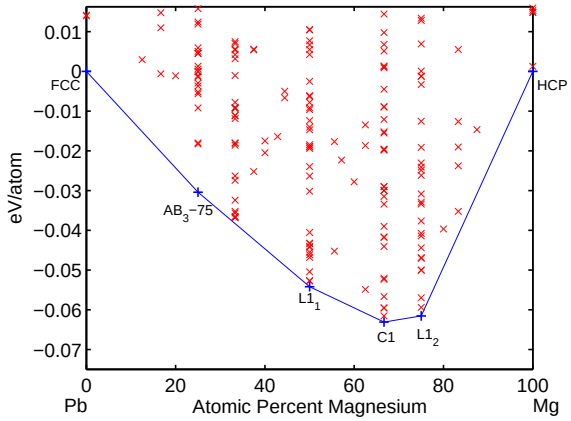

FIG. 11. Mg-Pb convex hull.

Mg-Pd *(Magnesium-Palladium)*

Pd-rich compounds have not been identified in the Mg-Pd system. Five Pd-rich *ab initio* compounds are predicted, however: $MgPd_7$-Ca_7Ge, $MgPd_4$-$D1_a$, $MgPd_3$-$D0_{23}$, $MgPd_2$-C37 and Mg_3Pd_5-Ga_3Pt_5.

Two experimental phases have been identified near composition MgPd: $L1_0$ forms slightly off stoichiometry at composition $Mg_{0.9}Pd_{1.1}$ and is the only intermediate phase to melt congruently. The B2 phase forms as MgPd and undergoes a peritectic decomposition at ∼700°C. The *ab initio* formation energies of these phases suggest that the $L1_0$ phase is the low temperature ground state, although the difference in energy is not considerable.

At composition Mg_3Pd, the experimental phase $D0_{18}$ is found above the tie line, $D0_{21}$ being the stable phase. There is one additional phase, $D0_{11}$, predicted with formation energy lower than $D0_{18}$. Entropic effects may account for the stability of $D0_{18}$ at finite temperature.

Crystallographic data was not available for the phase at composition Mg_4Pd. Furthermore, the $Mg_{85}Pd_{14}$ (cF396, #216) phase was excluded due to a large unit cell size and partial occupation of sites. *Ab initio* results

are thus inconclusive from composition ~Mg_4Pd.

Mg-Pd system

Comparison of low temperature phases		
Composition % Mg	Experimental results[21,104]	*Ab initio* results (Fig. 12)
12.5	*two-phase region*	Ca_7Ge
20.0	*two-phase region*	$MgPd_4$-$D1_a$
25.0	*two-phase region*	$MgPd_3$-$D0_{23}$ $D0_{22}$ ~8.2 meV/atom *above* $D0_{23}$
33.3	*two-phase region*	$MgPd_2$-C37
37.5	*two-phase region*	Ga_3Pt_5
50.0	MgPd-B2/$L1_0$	$L1_0$ B2 ~1.8 meV/atom *above* $L1_0$
66.6	*two-phase region*	$NiTi_2$/C16
~71.4	Mg_5Pd_2-$D8_{11}$	$D8_{11}$
75.0	Mg_3Pd-$D0_{18}$	$D0_{21}$ $D0_{11}$ ~7.6 meV/atom $D0_{18}$ ~19.4 meV/atom *above* $D0_{21}$
80.0	Mg_4Pd *unknown*	*two-phase region* $D1_a$ ~53.9 meV/atom *above tie line*
~85.7	$Mg_{85}Pd_{14}$	***

TABLE XIV: The Mg-Pd system.

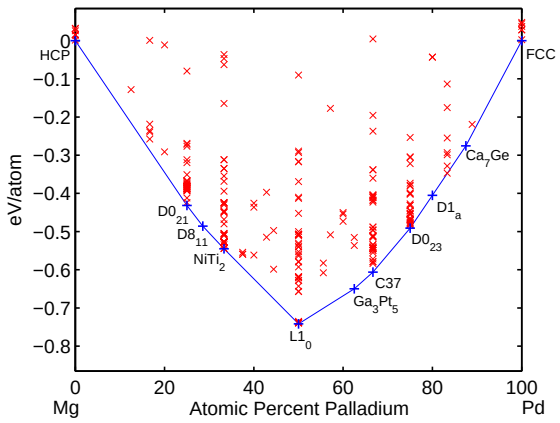

FIG. 12. Mg-Pd convex hull.

Mg-Pt *(Magnesium-Platinum)*

The phase diagram has not been determined for the Mg-Pt system. The experimental phases at compositions $MgPt_7$ and $Mg_{85}Pt_7$ were not evaluated because the structures have not been completely determined. Nevertheless, the *ab initio* ground state Ca_7Ge is somewhat consistent with what is known about the experimental phase at $MgPt_7$: Ca_7Ge is a doubling of the $L1_2$ structure when the 4b Wyckoff position is replaced by a Ge atom, and the experimental phase at $MgPt_7$ has been reported to consist of eight $L1_2$-type cells[21,105].

At compositions Mg_2Pt and $MgPt_2$, phases may exist where none have been experimentally observed. While the $MgPt_2$-Ga_2Hf structure is found slightly above the tie line (~1.9 meV), the C16 structure is stable at Mg_2Pt. We are unable to explain the surprisingly high *ab initio* energy of the MgPt-B20 phase, as well as the relative stabilities of Mg_3Pt-$D0_{21}$, -$D0_{11}$, and -$D0_{18}$ that are in contradiction to experiment. It is interesting to note, however, that an identical ordering of the phases at composition Mg_3Pt occurs in the chemically similar Mg-Pd system, and that the stable *ab initio* and experimental phase at composition MgPd is $L1_0$.

Mg-Pt system

Comparison of low temperature phases		
Composition % Mg	Experimental results[105,106]	*Ab initio* results (Fig. 13)
12.5	$MgPt_7$ *unknown*	Ca_7Ge
25.0	$MgPt_3$-$L1_2$	$L1_2$
33.3	—	Ga_2Hf ~1.9 meV *above tieline*
50.0	MgPt-B20	MgPt-$L1_0$ NiTi ~23.9 meV/atom B2 ~31.2 meV/atom B20 ~149.2 meV/atom *above* $L1_0$
66.6	—	Mg_2Pt-C16 $NiTi_2$ ~10.7 meV/atom *above* C16
75.0	Mg_3Pt-$D0_{18}$	Mg_3Pt-$D0_{21}$ $D0_{11}$ ~12.0 meV/atom $D0_{18}$ ~18.5 meV/atom *above* $D0_{21}$
~85.7	$Mg_{85}Pt_{14}$	***

TABLE XV: The Mg-Pt system.

Mg-Rh *(Magnesium-Rhodium)*

Although the phase diagram has not been determined for the Mg-Rh system, three experimental phases have been observed: MgRh-B2, Mg_5Rh_{2-x}-Al_5Co_2 and $Mg_{44}Rh_7$. The experimental phases are confirmed by *ab initio* calculations. Additional *ab initio* phases are found at compositions, $MgRh_7$, $MgRh_3$, and Mg_2Rh with structures described in the table.

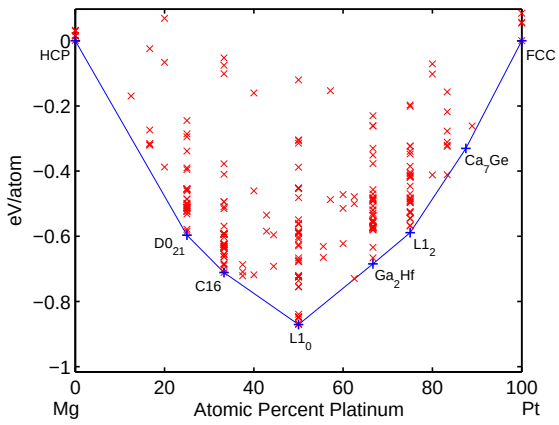

FIG. 13. Mg-Pt convex hull.

Mg-Rh system

Comparison of low temperature phases		
Composition % Mg	Experimental results[21]	*Ab initio* results (Fig. 14)
12.5	—	Ca_7Ge
25.0	—	$Re_3Ru^\star$-124[†] $MgRh_3$-$D0_{22}$ ∼30 meV/atom *above* $Re_3Ru^\star$-124
50.0	MgRh-B2	B2
66.6	—	$Hf_2Tl^\star$-6[†,b] $NiTi_2$ ∼17.8 meV/atom *above* Hf_2Tl-6*
∼71.4	Mg_5Rh_2-Al_5Co_2	Al_5Co_2
75.0	—	Mg_3Rh-$D0_{21}$
∼86.3	$Mg_{44}Rh_7$	$Mg_{44}Rh_7$

TABLE XVI: The Mg-Rh System. (†) See Structure Table 2 for crystallographic description. (b) Tetragonal distortion of β_2[10].

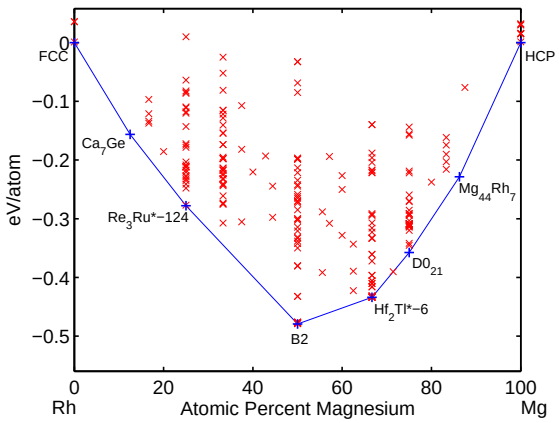

FIG. 14. Mg-Rh convex hull.

Mg-Ru *(Magnesium-Ruthenium)*

Very little published data exists for the Mg-Ru system. The phase diagram has not been determined. Two experimental intermetallic phases are observed: Mg_3Ru_2-A13 and $Mg_{44}Rh_7$. The latter phase is not entirely determined[21] but a rough *ab initio* evaluation of the prototype produces a thermodynamic minimum. An *ab initio* ground state is found at composition Mg_3Ru_2 with the A13 structure.

Mg-Ru system

Comparison of low temperature phases		
Composition % Mg	Experimental results[21]	*Ab initio* results (Fig. 15)
60.0	Mg_3Ru_2-A13	A13
∼86.3	$Mg_{44}Rh_7$	$Mg_{44}Rh_7$

TABLE XVII: The Mg-Ru system.

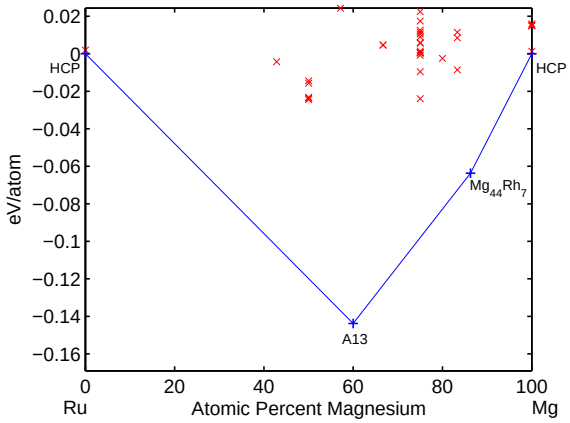

FIG. 15. Mg-Ru convex hull.

Mg-Sc *(Magnesium-Scandium)*

The phase diagram for the Mg-Sc system has not been completely determined. *Ab initio* predictions of stable phases differ slightly from data reported in experimental phase diagrams. A single intermetallic compound, MgSc-B2, is reported by experiment while three *ab initio* phases exist. The B2 phase has a slightly higher formation energy at T=0 K than the *ab initio* ground state, B11. The two additional *ab initio* phases are $MgSc_2$-C49 and Mg_3Sc-$D0_{19}$.

Mg-Sc system		
Comparison of low temperature phases		
Composition % Mg	Experimental results[21,107]	*Ab initio* results (Fig. 16)
33.3	*two-phase region*	$MgSc_2$-C49 $\beta 2$ ($FCC^{[100]}_{AB2}$) ~3.9 meV/atom *above* C49
50.0	MgSc-B2	B11 B2 ~5.9 meV/atom *above* B11
75.0	*two-phase region*	Mg_3Sc-$D0_{19}$ $L1_2$ ~2.0 meV/atom *above* $D0_{19}$

TABLE XVIII: The Mg-Sc system.

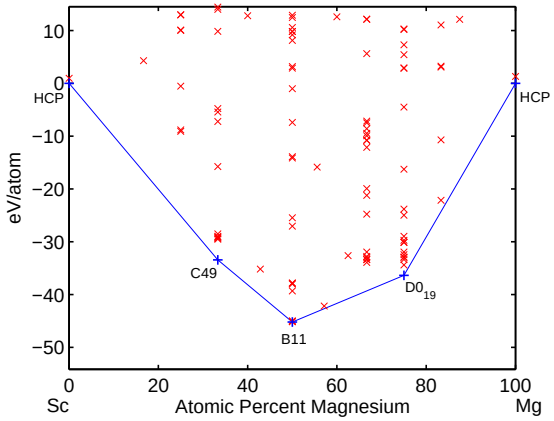

FIG. 16. Mg-Sc convex hull.

Mg-Si *(Magnesium-Silicon)*

Stability of the experimental compound, Mg_2Si-C1, is corroborated by *ab initio* calculations. The clarity with which the single *ab initio* prediction arises in this system is consistent with the well-established nature of the Mg-Si system.

Mg-Si system		
Comparison of low temperature phases		
Composition % Mg	Experimental results[21,108–114]	*Ab initio* results (Fig. 17)
66.6	Mg_2Si-C1	C1

TABLE XIX: The Mg-Si system.

Mg-Sn *(Magnesium-Tin)*

A single *ab initio* ground state exists in the Mg-Sn system and occurs at the same composition and with the same structure (Mg_2Sn-C1) as the experimental compound.

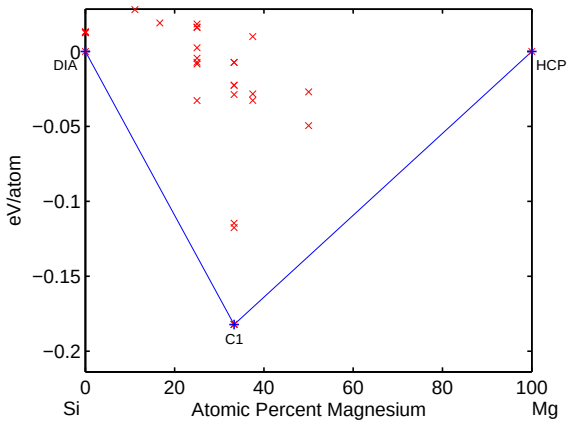

FIG. 17. Mg-Si convex hull.

Mg-Sn system		
Comparison of low temperature phases		
Composition % Mg	Experimental results[21,115–125]	*Ab initio* results (Fig. 18)
66.6	Mg_2Sn-C1	C1

TABLE XX: The Mg-Sn system.

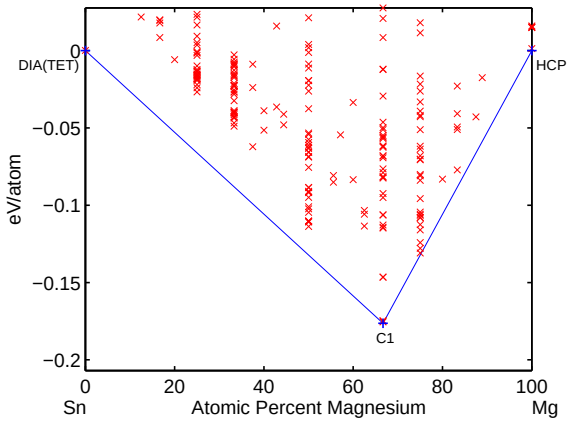

FIG. 18. Mg-Sn convex hull.

Mg-Sr *(Magnesium-Strontium)*

Intermetallic compounds in the Mg-Sr system form only at Mg-rich compositions. Four experimental phases have been observed: Mg_2Sr-C14, $Mg_{23}Sr_6$-$D8_a$, $Mg_{38}Sr_9$, and $Mg_{17}Sr_2$. *Ab initio* ground states generally agree with experiment. The phase at composition $Mg_{38}Sr_9$ (hP94, #194) is described by a large unit cell is above the tie line. It should be noted also that the specification of this phase is not completely unambiguous[21].

Mg-Sr system		
Comparison of low temperature phases		
Composition % Mg	Experimental results[21,126]	*Ab initio* results (Fig. 19)
66.6	Mg_2Sr-C14	C14 C36 ∼1.9 meV/atom *above* C14
∼79.3	$Mn_{23}Th_6$	$Mn_{23}Th_6$
∼80.9	$Mg_{38}Sr_9$	$Mg_{38}Sr_9$ ∼10.4 meV/atom *above tie line*
∼89.5	$Ni_{17}Th_2$	$Ni_{17}Th_2$

TABLE XXI: The Mg-Sr system.

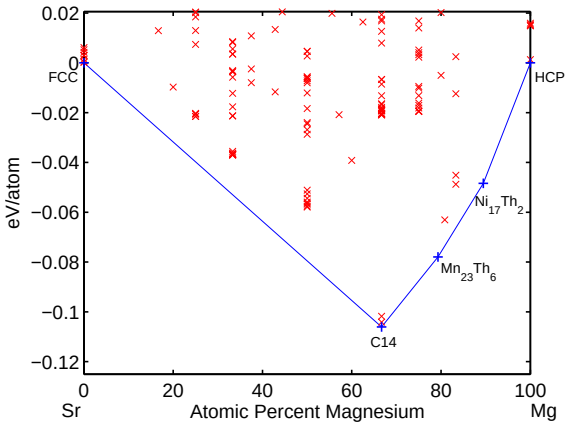

FIG. 19. Mg-Sr convex hull.

Mg-Tc *(Magnesium-Technetium)*

Little published phase data exists for the Mg-Tc system and no compounds have been reported[21]. *Ab initio* compounds are predicted: $MgTc_2$-C11$_b$, Mg_3Tc_4, and MgTc-B11.

Mg-Tc system		
Comparison of low temperature phases		
Composition % Mg	Experimental results	*Ab initio* results (Fig. 20)
33.3	—	$MgTc_2$-C11$_b$ ∼-15.8 meV/atom
∼42.9	—	Cu_4Ti_3 ∼-20.2 meV/atom
50.0	—	MgTc-B11 ∼-22.4 meV/atom

TABLE XXII: The Mg-Tc system.

Mg-Y *(Magnesium-Yttrium)*

Ab initio phases are predicted in general agreement with the experimental phases found in the Mg-Y system (MgY-B2, Mg_2Y-C14, and $Mg_{24}Y_5$-A12). The Laves phase polytypes, C15, C36, and C14 are within ∼2 meV of each other and are near, although slightly above, the thermodynamic minimum (B2↔D0$_3$). The C15 phase has the lowest formation energy and is ∼2 meV above

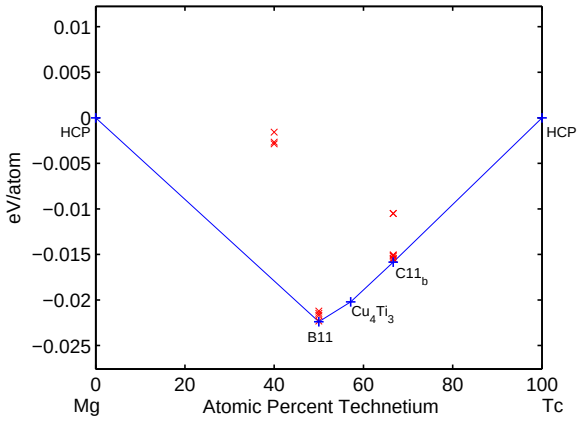

FIG. 20. Mg-Tc convex hull.

the tie line. The $Mg_{24}Y_5$-A12 phase is similarly near, although slightly above, the thermodynamic minimum (D0$_3$ ↔Mg-A3). However, because this "metastability" is small compared to the total energies of the system, it is reasonable to consider these as the low temperature ground state predictions for this system.

Additional *ab initio* phases are predicted where no experimental phases have been observed. An Y-rich phase with the C49 structure and a Mg-rich phase with the D0$_3$ structure are stable.

Mg-Y system		
Comparison of low temperature phases		
Composition % Mg	Experimental results[21,127–133]	*Ab initio* results (Fig. 21)
33.3	*two-phase region*	MgY_2-C49
50.0	MgY-B2	B2
66.6	Mg_2Y-C14	C15/C36/C14 ∼2 meV *above tie line*
75.0	*two-phase region*	Mg_3Y-D0$_3$ D0$_{19}$ ∼2.5 meV/atom *above* D0$_3$
∼82.8	$Mg_{24}Y_5$-A12	*two-phase region* A12 ∼3.8 meV/atom *above tie line*

TABLE XXIII: The Mg-Y system.

Mg-Zn *(Magnesium-Zinc)*

The low temperature phases of the Mg-Zn system are not completely determined. In particular there is some ambiguity in the specification of low temperature phases at compositions MgZn and ∼Mg_4Zn_7.

An unobserved Mg-rich phase is predicted, Mg_2Zn-C16, and there is no stable phase at composition MgZn, although the B33 structure is close to the tie line (∼8.0 meV/atom above C14 ↔ C16). The Mg_4Zn_7 phase (mS110, #12) is also thermodynamically unstable (∼11.8

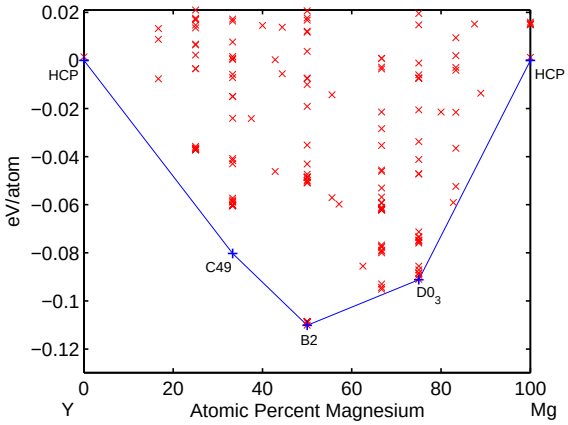

FIG. 21. Mg-Y convex hull.

meV above the tie line C14 ↔ C16). The experimental phases with structures $D8_c$ and C14 are corroborated by the existence of the same *ab initio* ground states.

Mg-Zn system

Comparison of low temperature phases		
Composition % Mg	Experimental results[21,134–145]	*Ab initio* results (Fig. 22)
∼15.3	Mg_2Zn_{11}-$D8_c$	$D8_c$
33.3	$MgZn_2$-C14	C14
∼36.3	Mg_4Zn_7	*two-phase region* Mg_4Zn_7 ∼11.8 meV/atom *above tie line*
50.0	MgZn *(unknown)*	*two-phase region* MgZn-B33 ∼8.0 meV/atom *above tie line.*
66.6	*two-phase region*	Mg_2Zn-C16

TABLE XXIV: The Mg-Zn system.

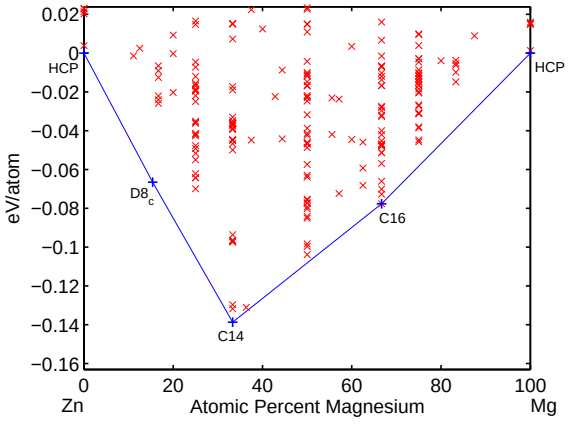

FIG. 22. Mg-Zn convex hull.

Mg-Zr *(Magnesium-Zirconium)*

The Mg-Zr system has been investigated in the Mg-rich region (0 to 1 at. % Zr) with consensus regarding the existence of a peritectic reaction at ∼1 at. % Zr[21,146–148]. The existence of intermediate phases, however, has not been verified and reports of such are believed to be due to impurities[21]. Nevertheless, two stable compounds are predicted by *ab initio* calculations: Mg_3Zr_4-Cu_4Ti_3 and MgZr-B11.

Mg-Zr system

Comparison of low temperature phases		
Composition % Mg	Experimental results[21]	*Ab initio* results (Fig. 23)
∼42.9	*non-compound-forming*	Mg_3Zr_4-Cu_4Ti_3
50.0	*non-compound-forming*	MgZr-B11

TABLE XXV: The Mg-Zr system. (†) See Structure Tables for crystallographic description.

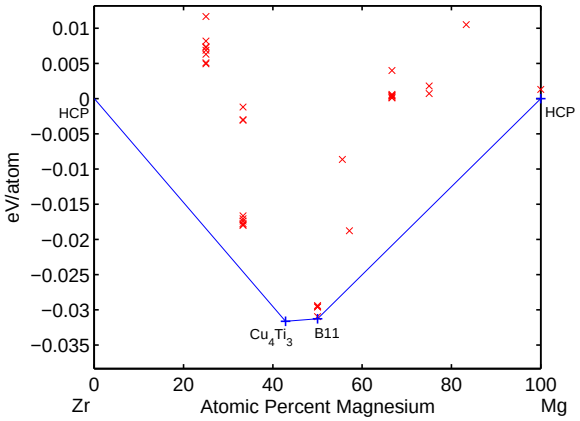

FIG. 23. Mg-Zr convex hull.

IV. CONCLUSION

Using the AFLOW HT framework, we have explored the full composition range of 34 Mg-X binary systems at $T = 0$ K. As described in "Method", the accuracy of the method, η_c, can be estimated within upper and lower bounds, $86.0\% \leq \eta_c \leq 98.2\%$. In that analysis, we did not include those cases for which *ab initio* phases exist *in addition* to experimental phases. Such occurrences are frequent (found in a little more than one-third of systems) and offer opportunities for new alloy design. Also of interest are the non-compound-forming systems Mg-Na, Mg-Tc, and Mg-Zr with thermodynamically stable structures. These offer particularly intriguing avenues for further investigation (see Table II).

The considerable agreement between *ab initio* predictions and experimental phases is encouraging from

the standpoint of first-principles viability as a paradigm for alloy design and exploration. The first-principles methodology used here (in particular, the pseudopotential approach to atomic interactions) is seldom pushed to the extent required by this study. Even so, the accurate prediction of experimental phases is well maintained, giving credence to *ab initio* predictions *not* corroborated by experiment.

It should be emphasized also that when *ab initio* phases contradict experiment we cannot immediately come to the conclusion of error on the part of the method. Deficiencies in the experimental characterization of binary systems exist due to the significant challenges associated with mixing alloys (e.g., impurities, kinetics). These limitations must be considered when any attempt at comparing *ab initio* ground states to experimental phases is made.

Finally, whether differences in the predictions of ground states by *ab initio* calculations are due to the limitations of first-principles methods themselves or experiment (in fact, it is unlikely to be entirely one or the other), the direction of future experiments, especially those probing difficult to reach regions of the binary alloy landscape, should be aided by the data presented in this work. Many avenues for further investigation are clearly presented. As examples, we mention the non-Mg-rich phases predicted in Ir-Mg, Mg-Pb, Mg-Pd, Mg-Rh, and the non-compound-forming systems with *ab initio* phases mentioned previously.

Acknowledgment. We thank Wahyu Setyawan, Ohad Levy, Junkai Xue, Shidong Wang and Mike Mehl for fruitful discussions. The research was supported by ONR (N00014-07-1-0878, N00014-07-1-1085, and N00014-09-1-0921) and NSF (DMR-0639822 and DMR-0650406). We are grateful for extensive use of the Fulton Supercomputing Lab at Brigham Young University and Teragrid resources (MCA-07S005).

[1] G. L. W. Hart and R. W. Forcade, Phys. Rev. B **77**, 224115 (2008).
[2] U. S. Energy Information Administration, *Annual Energy Review 2009*, DOE/EIA-0384 (2009).
[3] H. Zhang, S. Shang, J. Saal, A. Saengdeejing, Y. Wang, L.-Q. Chen, and Z.-K. Liu, Intermetallics **17**, 878 (2009).
[4] S. Ganeshan, S. L. Shang, H. Zhang, Y. Wang, M. Mantina, and Z.-K. Liu, Intermetallics **17**, 313 (2009).
[5] S. Curtarolo, D. Morgan, and G. Ceder, Calphad **29**, 163 (2005).
[6] S. Curtarolo, D. Morgan, K. Persson, J. Rodgers, and G. Ceder, Phys. Rev. Lett. **91**, 135503 (2003).
[7] S. Curtarolo, G. L. W. Hart, W. Setyawan, M. Mehl, M. Jahnatek, R. V. Chepulskii, O. Levy, and D. Morgan, *"AFLOW: software for high-throughput calculation of material properties"*, http://materials.duke.edu/aflow.html (2010).
[8] S. Curtarolo, W. Setyawan, G. L. W. Hart, M. Jahnatek, R. V. Chepulskii, R. H. Taylor, S. Wang, J. Xue, K. Yang, O. Levy, et al., submitted, Comp. Mat. Sci. (2011).
[9] O. Levy, G. L. W. Hart, and S. Curtarolo, J. Am. Chem. Soc. **132**, 4830 (2010).
[10] O. Levy, G. L. W. Hart, and S. Curtarolo, Acta Mater. **58**, 2887 (2010).
[11] R. H. Taylor, S. Curtarolo, and G. L. W. Hart, Phys. Rev. B **81**, 024112 (2010).
[12] R. Taylor, S. Curtarolo, and G. L. W. Hart, J. Am. Chem. Soc. **132**, 6851 (2010).
[13] O. Levy, G. L. W. Hart, and S. Curtarolo, Phys. Rev. B **81**, 174106 (2010).
[14] G. L. W. Hart and R. W. Forcade, Phys. Rev. B **80**, 014120 (2009).
[15] G. Kresse and J. Hafner, Phys. Rev. B **47**, 558 (1993).
[16] G. Kresse and D. Joubert, Phys. Rev. B **59**, 1758 (1999).
[17] J. P. Perdew, K. Burke, and M. Ernzerhof, Phys. Rev. Lett. **77**, 3865 (1996).
[18] A. N. Kolmogorov and S. Curtarolo, Phys. Rev. B **73**, 180501(R) (2006).
[19] A. N. Kolmogorov and S. Curtarolo, Phys. Rev. B **74**, 224507 (2006).
[20] P. Villars, M. Berndt, K. Brandenburg, K. Cenzual, J. Daams, F. Hulliger, T. Massalski, H. Okamoto, K. Osaki, A. Prince, et al., J. Alloys Compound. **367**, 293 (2004).
[21] T. B. Massalski, H. Okamoto, P. R. Subramanian, and L. Kacprzak, eds., *Binary alloy phase diagrams* (American Society for Metals, Materials Park, OH, 1990).
[22] S. Curtarolo, A. N. Kolmogorov, and F. H. Cocks, Calphad **29**, 155 (2005).
[23] J. P. Perdew and Y. Wang, Phys. Rev. B **45**, 13244 (1992).
[24] P. Blaha, *WIEN2K An Augmented Plane Wave+Local Orbitals Program For Calculating Crystal Properties* (Karlheintz Schwarz, Techn. Univ., Wien, Austria, 2001), ISBN 3-9501031-1-2.
[25] Y. Zuo and Y. Chang, Calphad **17**, 161 (1993).
[26] N. Saunders, Calphad **14**, 61 (1990).
[27] E. Schürmann and R. Engel, Giessereiforschung **38**, 58 (1986).
[28] Y. Minamino, T. Yamane, T. Miyake, M. Koizumi, and Y. Miyamoto, Materials Science and Technology **2**, 777 (1986).
[29] H. J. Voss and E. Schürmann, Giessereiforschung **33**, 43 (1981).
[30] E. Schürmann and I. K. Geissler, Giessereiforschung **32**, 167 (1980).
[31] M. L. Saboungi and C. C. Hsu, Calphad **1**, 237 (1977).
[32] E. Schürmann and A. Fischer, Giessereiforschung **29**, 107 (1977).
[33] W. Wachtel, S. Woerner, and S. Steeb, Z. Metallkd. **56**, 776 (1965).
[34] K. A. Bolshakov, P. I. Fedorov, and E. I. Smarina, Russian Journal of Inorganic Chemisty, translated from Zhurnal Neorganicheskoi Khimii **8**, 734 (1963).
[35] J. B. Clark and F. N. Rhines, Transactions of the American Institute of Mining, Metallurgical and Petroleum Engineers **209**, 6 (1957).
[36] K. Übersicht, K. Eickhoff, and H. Vosskühler, Z. Metallkd. **44**, 223 (1953).
[37] M. I. Zakharova and V. A. Il'ina, Zhurnal Fizicheskoi Khimii **24**, 714 (1950).
[38] K. Little, H. J. Axon, and W. Hume-Rothery, J. Inst. Met. **75**, 39 (1948-49).
[39] E. Butchers and W. Hume-Rothery, J. Inst. Met. **71**, 291 (1945).
[40] W. Köster and E. Wagner, Z. Metallkd. **30**, 338 (1938).
[41] W. Hume-Rothery and G. V. Raynor, J. Inst. Met. **63**, 201 (1938).
[42] W. L. Fink and L. A. Willey, Transactions of the American Institute of Mining, Metallurigical and Petroleum Engineers **124**, 78 (1937).
[43] C. Goria and G. Venturello, Gazzetta Chimica Italiana **67**, 487 (1937).
[44] J. L. Haughton and R. J. M. Payne, J. Inst. Met. **57**, 287 (1935).
[45] P. Saldau and M. Zamotorin, J. Inst. Met. **48**, 221 (1932).
[46] G. Siebel and E. Schmid, Z. Metallkd. **23**, 202 (1931).
[47] D. Hanson and M. L. V. Gayler, J. Inst. Met. **26**, 321 (1921).
[48] D. Hanson and M. L. V. Gayler, J. Inst. Met. **24**, 201 (1920).
[49] R. Vogel, Angewandte Chemie **35**, 705 (1922).
[50] G. G. Urasow, Z. Anorganische Chemie **64**, 375 (1909).
[51] R. Vogel, Z. Anorganische Chemie **63**, 169 (1909).
[52] A. Renu, L. J. Joong, H. L. Lukas, and F. Sommer, Z. Metallkd. **86**, 103 (1995).
[53] W. Klemm and F. Dinkelacker, Z. Anorganische Chemie **255**, 2 (1947).
[54] W. Bulian and E. Fahrenhorst, Z. Metallkd. **37**, 70 (1946).
[55] H. Nowotny, E. Wormnes, and A. Mohrnheim, Z. Metallkd. **32**, 39 (1940).
[56] H. Vosskühler, Z. Metallkd. **29**, 236 (1937).
[57] J. L. Haughton, J. Inst. Met. **61**, 241 (1937).
[58] N. Baar, Z. Anorganische Chemie **70**, 352 (1911).
[59] M. Asta, R. McCormack, and D. D. de Fontaine, Phys. Rev. B **48**, 748 (1993).
[60] M. Asta, R. McCormack, and D. D. Fontaine, Giessereiforschung **36**, 53 (1984).
[61] R. Castanet, Z. Moser, and W. Gasior, Calphad **4**, 231 (1980).
[62] G. Fischer, D. Godel, and S. Steeb, Z. Metallkd. **64**, 200 (1973).
[63] P. C. Frantz and M. Gantois, Journal of Applied Crystal-

lography **4**, 387 (1971).
[64] C. Frantz, M. Gantois, and A. Pianelli, Comptes Rendus Hebdomandaires des Seances de l'Academie des Sciences **265**, 1019 (1967).
[65] S. B. Felgina, Russian Metallurgy and Mining **6**, 96 (1964).
[66] O. Kubaschewski and T. G. Chart, J. Inst. Met. **93**, 329 (1964-65).
[67] J. B. Newkirk, Transactions of the American Institute of Mining, Metallurgical and Petroleum Engineers **200**, 673 (1954).
[68] W. Hume-Rothery and G. V. Raynor, Proceedings of the Royal Society of London **174**, 471 (1940).
[69] W. Köster and E. Wagner, Z. Metallkd. **30**, 335 (1938).
[70] E. Jünecke, Z. Metallkd. **30**, 424 (1938).
[71] G. Grube and E. Schiedt, Z. Anorganische und Allgemeine Chemie **194**, 190 (1930).
[72] W. Hume-Rothery and S. W. Rowell, J. Inst. Met. **38**, 137 (1927).
[73] G. Bruni and C. Sandonnini, Z. Anorganische Chemie **78**, 273 (1912).
[74] G. Grube, Z. Anorganische Chemie **49**, 72 (1906).
[75] Y. Zuo and Y. A. Chang, Z. Metallkd. **84**, 662 (1993).
[76] C. A. Coughanowr, I. Ansara, R. Luoma, M. Hamalainen, and H. L. Lukas, Z. Metallkd. **82**, 574 (1991).
[77] P. Bagnoud and P. Feschotte, Z. Metallkd. **69**, 114 (1978).
[78] W. R. D. Jones, J. Inst. Met. **46**, 395 (1931).
[79] O. Dahl, Wissenschaftliche Veröffentlichungen aus den Siemens Werken **6**, 222 (1927).
[80] Y. K. Rao and G. R. Belton, Metallurgical Transactions **2**, 2215 (1971).
[81] R. Geffken and E. Miller, Transactions of the Metallurgical Society of AIME **242**, 2323 (1968).
[82] H. Westlinning and W. Klemm, Z. Anorganische und Allgemeine Chemie **245**, 365 (1941).
[83] G. V. Raynor, J. Inst. Met. **66**, 403 (1940).
[84] F. A. Calvo and M. P. Hierro, Revista de Metalurgia (Madrid) **23**, 333 (1987).
[85] W. Klemm, **62**, 133 (1950).
[86] H. Nowotny, Z. Metallkd. **37**, 130 (1946).
[87] L. B. Hunt, Platinum Metals Review **31**, 32 (1987).
[88] R. Ferro, G. Rambaldi, and R. Capelli, Journal of the Less-Common Metals **4**, 16 (1962).
[89] M. Giovannini, A. Saccone, R. Marazza, and R. Ferro, Metallurgical Transactions, Section A: Physical Metallurgy and Materials Science **26**, 5 (1995).
[90] P. Manfrinetti and K. J. Gschneidner, Journal of the Less-Common Metals **123**, 267 (1986).
[91] R. Joseph and K. J. Gschneidner, Transactions of the Metallurgical Society of AIME **233**, 2063 (1965).
[92] S. Felgina, Russian Metallurgy and Mining **6**, 96 (1964).
[93] R. Vogel and T. Heumann, Z. Metallkd. **38**, 1 (1947).
[94] F. Weibke and W. Schmidt, Zeitschrift für Elektrochemie und Angewandte Physikalische Chemie **46**, 357 (1940).
[95] H. Abe, K. Ito, and T. Suzuki, Acta Metallurgica **18**, 991 (1970).
[96] C. D. G. Jr., J. A. Burgo, J. W. Cooper, C. L. Douglas, P. S. Gilman, W. T. Kelley, and A. Nagelberg, Metallurgical Transactions **2**, 2964 (1971).
[97] J. M. Eldridge, E. Miller, and K. L. Komarek, Transactions of the Metallurgical Society of AIME **233**, 1303 (1965).
[98] G. W. Horsley and J. T. Maskrey, J. Inst. Met. **86**, 446 (1957-58).
[99] F. Foote and E. R. Jette, Petroleum Engineers **143**, 124 (1941).
[100] G. V. Raynor, J. Inst. Met. **66**, 403 (1940).
[101] H. Vosskühler, Z. Metallkd. **31**, 109 (1939).
[102] J. Goebel, Z. Metallkd. **14**, 357 (1922).
[103] N. S. Kurnakow and N. J. Stepanow, Z. Anorganische Chemie **46**, 177 (1905).
[104] E. M. Savitskii, V. F. Terekhova, and N. A. Birun, Russian Journal of Inorganic Chemistry **7**, 1228 (1962).
[105] W. Bronger and W. Klemm, Z. Anorganische und Allgemeine Chemie **319**, 58 (1962).
[106] A. A. N. Hashemi and J. B. Clark, Bulletin of Alloy Phase Diagrams **6**, 534 (1985).
[107] B. J. Beaudry and A. H. Daane, Journal of the Less-Common Metals **18**, 305 (1969).
[108] D. Lüdecke, Z. Metallkd. **77**, 278 (1986).
[109] P. Dörner, H. Kreig, H. L. Lukas, R. Müller, and G. Petzow, Calphad **5**, 41 (1981).
[110] E. Schürmann and A. Fischer, Giessereiforschung **29**, 111 (1977).
[111] R. Geffken and E. Miller, Transactions of the Metallurgical Society of AIME **242**, 2323 (1968).
[112] G. V. Raynor, J. Inst. Met. **66**, 403 (1940).
[113] B. E. H. Sawamoto, Suiyokwai-Shi (Transactions of the Mining and Metallurgical Association Kyoto) **8**, 713 (1935).
[114] R. Vogel, Z. Anorganische Chemie **61**, 46 (1909).
[115] S. Srinivasan, Z. Metallkd. **82**, 841 (1991).
[116] B. Jönsson and J. Ågren, Metallurgical Transactions, Section A: Physical Metallurgy and Materials Science **17**, 607 (1986).
[117] L. M. Pavlova and K. B. Poyarkov, Russian Journal of Physical Chemistry **56**, 183 (1982).
[118] A. K. Nayak and W. Oelsen, Transactions of the Indian Institute of Metals **21**, 15 (1968).
[119] J. M. Eldridge, E. Miller, and K. L. Komarek, Transactions of the Metallurgical Society of AIME **236**, 114 (1966).
[120] S. B. Felgina, Russian Metallurgy and Mining **6**, 96 (1964).
[121] W. Wobst, Zeitschrift für Physikalische Chemie, Abteilung B **219**, 239 (1962).
[122] G. V. Raynor, J. Inst. Met. **66**, 403 (1940).
[123] W. Hume-Rothery, J. Inst. Met. **35**, 295 (1926).
[124] W. Hume-Rothery, Z. Anorganische Chemie **46**, 177 (1905).
[125] G. Grube, Z. Anorganische Chemie **46**, 76 (1905).
[126] W. Klemm and F. Dinkelacker, Z. Anorganische Chemie **255**, 2 (1947).
[127] Q. Ran, H. L. Lukas, G. Effenberg, and G. Petzow, Calphad **12**, 375 (1988).
[128] Z. A. Sviderskaya and E. M. Padezhnova, Russian Metallurgy **6**, 126 (1988).
[129] D. Miannay, P. Grégoire, P. Azou, and P. Bastien, Comptes Rendus Hebdomadaires des Seances de l'Academie des Sciences, Serie C: Sciences Chimiques **265**, 1107 (1967).
[130] J. F. Smith, D. M. Bailey, D. B. Novotny, and J. E. Davison, Acta Metallurgica **13**, 889 (1965).
[131] I. L. Markova, V. F. Terekhova, and E. M. Savitskii, Voprosy Teorii i Primeneniya Redkozemel'nykh Metallov pp. 124–128 (1964).
[132] D. Mizer and J. B. Clark, Transactions of the American Institute of Mining, Metallurgical and Petroleum Engi-

neers **221**, 207 (1961).
[133] E. D. Gibson and O. N. Carlson, Transactions of the American Society for Metals **52**, 1084 (1960).
[134] T. Gödecke and F. Sommer, Z. Metallkd. **85**, 683 (1994).
[135] R. Agarwal, S. G. Fries, H. L. Lukas, G. Petzow, F. Sommer, T. G. Chart, and G. Effenberg, Z. Metallkd. **83**, 216 (1992).
[136] M. E. Drits, Z. A. Sviderskaya, E. S. Kadaner, and S. B. Felgina, Russian Metallurgy and Mining **5**, 90 (1963).
[137] K. P. Adnerko, E. J. Klimek, D. W. Levinson, and W. Rostoker, Transactions of the American Society of Metals **49**, 778 (1957).
[138] J. B. Clark and F. N. Rhines, Transactions of the American Institute of Mining, Metallurgical and Petroleum Engineers **209**, 425 (1957).
[139] W. Klemm, Angewandte Chemie **62**, 133 (1950).
[140] F. Laves, Naturwissenschaften **27**, 454 (1939).
[141] W. Hume-Rothery and E. O. Rounsefell, J. Inst. Met. **41**, 119 (1929).
[142] R. Chadwick, J. Inst. Met. **39**, 285 (1928).
[143] G. Bruni and C. Sandonnini, Z. Anorganische Chemie **78**, 273 (1912).
[144] I. Mitteilung, G. Bruni, C. Sandonnini, and E. Quercigh, Z. Anorganische Chemie **68**, 73 (1910).
[145] G. Grube, Z. Anorganische Chemie **49**, 72 (1906).
[146] R. Arroyave, D. Shin, and Z.-K. Liu, Calphad **29**, 230 (2005).
[147] R. L. Crosby and K. A. Fowler (1962).
[148] I. M. Vesey and H. J. Bray, J. Inst. Met. **92**, 383 (1964).

System	Composition	Experimental results	*Ab initio* result	Details
Al-Mg	Al_2Mg	two-phase region	C14/C36	(b)
Au-Mg	Au_5Mg	solid solution	$HfPd_5$	(b)
	Au_3Mg_5	two-phase region	$D8_m$	(b)
Cd-Mg	$CdMg_2$	two-phase region	$InMg_2$	(d)
Hg-Mg	Hg_2Mg	$C11_b$	C_c	(d)
	Hg_2Mg_5	Hg_2Mg_5 *unknown*	two-phase region	(c)
	$HgMg_3$	$HgMg_3$	two-phase region	(d)
Ir-Mg	Ir_7Mg	—	Ca_7Ge	(b)
	Ir_3Mg	—	Re_3Ru^*-124	(b)
	IrMg	—	$FCC^{[311]}_{A2B2}$	(b)
	$IrMg_4$	$IrMg_4$ *unknown*	two-phase region	(c)
La-Mg	La_7Mg	two-phase region	Ca_7Ge	(b)
	$LaMg_{12}$	$LaMg_{12}$*unknown*	two-phase region	(b)
Mg-Na	Mg_3Na_2	non-compound-forming	Al_3Zr_2	(b)
Mg-Pb	$MgPb_3$	two-phase region	AB_3-75	(b)
	MgPb	two-phase region	$L1_1$	(b)
Mg-Pd	$MgPd_7$	two-phase region	Ca_7Ge	(b)
	$MgPd_4$	two-phase region	$D1_a$	(b)
	$MgPd_3$	two-phase region	$D0_{23}$	(b)
	$MgPd_2$	two-phase region	C37	(b)
	Mg_3Pd_5	two-phase region	Ga_3Pt_5	(b)
	Mg_2Pd	two-phase region	$NiTi_2$/C16	(d)
	Mg_3Pd	$D0_{18}$	$D0_{21}$	(d)
	Mg_4Pd	Mg_4Pd *unknown*	two-phase region	(c)
	$\sim Mg_6Pd$	$Mg_{85}Pd_{14}$ *unknown*	two-phase region	(e)
Mg-Pt	$MgPt_7$	$MgPt_7$ *unknown*	Ca_7Ge	(c)
	$MgPt_2$	—	Ga_2Hf	(b/d)
	MgPt	FeSi-B20	$L1_0$	(d)
	Mg_2Pt	—	C16	(b/d)
Mg-Rh	$MgRh_7$	—	Ca_7Ge	(b/d)
	$MgRh_3$	—	Re_3Ru^*-124	(b/d)
	Mg_2Rh	—	Hf_2Tl^*-6	(b/d)
	Mg_3Rh	—	$D0_{21}$	(b/d)
Mg-Ru	$Mg_{44}Rh_7$	$Mg_{44}Rh_7$	two-phase region	(c/e)
Mg-Sc	$MgSc_2$	two-phase region	C49	(b)
	Mg_3Sc	two-phase region	$D0_{19}/L1_2$	(b)
Mg-Sr	$Mg_{38}Sr_9$	$Mg_{38}Sr_9$	two-phase region	(b/e)
Mg-Tc	$MgTc_2$	non-compound-forming	$C11_b$	(b)
	Mg_3Tc_4	non-compound-forming	Cu_4Ti_3	(b)
	MgTc	non-compound-forming	B11	(b)
Mg-Y	MgY_2	two-phase region	C49	(d)
	Mg_3Y	two-phase region	$D0_3/D0_{19}$	(d)
	$Mg_{24}Y_5$	A12	two-phase region	(d/e)
Mg-Zn	Mg_4Zn_7	Mg_4Zn_7	two-phase region	(d/e)
	MgZn	unknown	two-phase region	(c)
	Mg_2Zn	two-phase region	C16	(b)
Mg-Zr	Mg_3Zr_4	non-compound-forming	Cu_4Ti_3	(b)
	MgZr	non-compound-forming	B11	(b)

TABLE XXVI: Summary of *ab initio*/experimental disagreements. A '—' indicates a system without an assessed phase diagram. (b) Discrepancy due to limited experimental data/System believed to be non-compound-forming. (c) Structural properties of experimental compound are not fully known. (d) *Ab initio* formation energy lower/higher than experimental phase energy alters tie line. (e) Experimental phase not (or only roughly) evaluated due to large cell size/partial occupation.

Compound	Be_2Zn-65$^{\star 13}$	Hf_5Pb-f63$^{\star 10}$	Hf_2Tl-6$^{\star 10}$
Lattice	orthorhombic	tetragonal	tetragonal
Space group	Fmmm #69	P4/mmm #123	I4/mmm #139
Pearson symbol	oF12	tP6	tI6
Primitive vect.	(SG option 2)	—	(SG option 2)
(a,b,c) (Å)	(3.780, 2.0978, 10.3)	(3.203,3.203,13.944)	(4.422,4.422,7.385)
(α,β,γ) (deg)	(90,90,90)	(90,90,90)	(90,72.577,90)
Wyckoff	(0,0,0.17832) 8i Be1	(0,0,-0.1794) 2g Hf1	(0,0,0.1746) 4e Hf1
positions	(0,0,1/2) 4b Zn1	(1/2,1/2,-0.3349) 2h Hf2	(0,0,1/2) 2b Tl2
	—	(0,0,1/2) 1b Hf3	—
	—	(1/2,1/2,0) 1c Pb1	—
AFLOW label	"549"	"477"	"547"
Compound	Mo_3Ti-81$^{\star 13}$	$HfPd_5$-f137$^{\star 10}$	Re_3Ru-124$^{\star 13}$
Lattice	orthorhombic	orthorhombic	orthorhombic
Space group	Immm #71	Cmmm #65	Imm2 #44
Pearson symbol	oI8	oS12	oI8
Primitive vect.	(4.444,3.173,8.971)	(11.998,4.0663,14.0723)	(9.005,2.757,4.775)
	(90,90,90)	(90,90,90)	(90,90,90)
Wyckoff	(0,0,0.2440) 4i Mo1	(0,0,0) 2a Hf1	(1/4,0,0) 4c Re1
positions	(0,1/2,0) 2d Mo2	(0.1663,0,1/2) 4h Pd1	(0,1/2,1/6) 2b Re2
	(1/2,0,0) 2b Ti1	(0.3369,0,0) 4g Pd2	(0,0,2/3) 2a Ru1
	—	(1/2,0,1/2) 2c Pd3	—
AFLOW label	"541"	"479"	"551"

TABLE XXVII: Crystallographic information for less familiar prototypes arising in our study. Atomic positions and unit cell parameters are fully relaxed (indicated by '*'). Corresponding unrelaxed structures are given in Table XXVIII.

Compound	Be_2Zn[13]	Hf_5Pb[10]	Hf_2Tl[10]	Re_3Ru[13]	Mo_3Ti[13]	$HfPd_5$[10]
Superlattice	bcc	fcc	fcc	hcp	bcc	hcp
Lattice	orthorhombic	tetragonal	tetragonal	orthorhombic	orthorhombic	orthorhombic
Space group	Fmmm #69	P4/mmm #123	I4/mmm #139	Imm2 #44	Immm #71	Cmmm #65
Pearson symbol	oF12	tP6	tI6	oI8	oI8	oS12
Primitive vect.						
$\mathbf{a}_1$/a	(0,1,2)	(1/2,1/2,0)	(3/2,0,-1/2)	(1/2,-$\sqrt{2}$/3,1.633)	(3/2,1/2,-1/2)	(1/2,3/2,1)
$\mathbf{a}_2$/a	(-1/2,3/2,3/2)	(0,3,3)	(3/2,0,1/2)	(-1/2,$\sqrt{2}$/3,1.633)	(1/2,3/2,1/2)	(0,3,3)
$\mathbf{a}_3$/a	(-1/2,-1/2,1/2)	(1/2,5/2,3)	(-3/2,-1/2,0)	(-1/2,-$\sqrt{2}$/3,-1.633)	(-1/2,-3/2,1/2)	(1/2,3/2,2)
Atomic Positions						
A1	(0,0,0)	(0,0,0)	(2/3,2/3,0)	(0,0,0)	(0,0,0)	(0,1/6,0)
A2	(2/3,2/3,1/3)	(0,1/6,0)	(1/3,1/3,0)	(1/2,1/2,0)	(1/4,3/4,1/2)	(0,1/3,0)
A3	—	(0,1/3,0)	—	(1/12,3/4,1/3)	(1/2,1/2,0)	(0,1/2,0)
A4	—	(0,1/2,0)	—	—	—	(0,2/3,0)
A5	—	(0,2/3,0)	—	—	—	(0,5/6,0)
B1	(1/3,1/3,2/3)	(0,5/6,0)	(0,0,0)	(7/12,1/4,1/3)	(3/4,1/4,1/2)	(0,0,0)
AFLOW label	"65"	"f63"	"6"	"124"	"81"	"f137"

TABLE XXVIII: Crystallographic data for unrelaxed prototypes reported in Table XXVIII.